Results in Physics 52 (2023) 106858

Contents lists available at ScienceDirect

Results in Physics

journal homepage: www.elsevier.com/locate/rinp

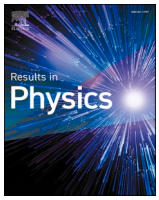

Effect of gamma ray on self-induced diffraction patterns of organic compound Poly (methyl-methacrylate films

Fadhil A. Tuma [a], Mohammed T. Obeed [a,b], Alyaa A. Jari [a], Hussain Ali Badran [a,*], T.A. Alaridhee [b]

[a] University of Basrah, Education College for Pure Sciences, Department of Physics, Basrah, Iraq
[b] University of Basrah, Polymer Research Center, Department of Material Science, Basrah, Iraq

ARTICLE INFO

Keywords:
Laser
Bleaching
Diffraction ring
Waviness, 2-NPb compound

ABSTRACT

Poly (methyl-methacrylate) (PMMA) doped organic compound (2-(2,3-dimethylphenyl-amino)-*N*-Phenyl benzamide) (2-NPb (films are produced on glass substrates with 5 μm thickness. The influence that gamma (γ) radiation has on the structure of the surface morphology of polymer films, the structure dependence of the optoelectronic properties and the optical properties of a prepared 2-NPb:PMMA film was studied under different doses (21, 42 and 64 KGy) of γ- rays emitted by a ^{137}Cs source with an exposure rate of 0.56 Gy/min. The surface morphology of the 2-NPb:PMMA film for un-irradiated and irradiated sample was studied using a microscope with a digital camera along with texture, waviness and roughenss analysis of the entire surface of the films. The optical properties, together with an in-depth analysis of the dispersion energies and parameters, optoelectrical characteristics, and certain nonlinear optical parameters were comprehensively examined and addressed. In addition, the study of optical properties also included some nonlinear optical parameters. Results show that by doping organic compound (2-NPb) in PMMA, the absorption spectra of samples are decreased and superficial morphology of the film has been affected by γ-rays. As the polymer film was irradiated with a continuous-solid state laser (Solid-State-Laser −532–100 T) beam of 532 nm, self-diffraction ring patterns were seen, and it was shown that the diffraction ring patterns rely heavily on ring numbers and radiation dosage. The nonlinear refractive index,n_2, for polymer film for un-irradiated and irradiated are estimated to be 0.23×10^{-6}, 0.92×10^{-6}, 1.64×10^{-6}, 3.14×10^{-6} cm^2/W, respectively due to diffraction ring patterns. The diffraction ring patterns that were acquired via experimentation are then numerically estimated by making use of the Fresnel-Kirchhoff diffraction integral. The results of these calculations have satisfactory qualitative and quantitative accords.

Introduction

When a powerful light beam interacts with a nonlinear material, it is possible to generate a wide variety of spatial effects [1–5]. In particular, a distribution scheme of the concentric ring intensity can be induced in the far-field of a beam after propagation across a non-linear material. When a powerful light beam traverses a nonlinear material, the pattern of intensity distributions over the rings produces effects like spatial phase modulation, It implies establishing a spatial distribution of laser energy that overlaps with the effective beam transmission that is the consequence of thermal factors [6,7]. In many different systems, such as vapor of some atoms, conducting polymers, thermo-tropic liquid crystals, and nano or micro-structured materials, the spatial phase modulation may be seen [8–10]. When a laser that emits a continuous wave is used, the thermal effects have a particularly large impact on the change in the material's refractive index [11–15]. The beam laser's profile distribution in terms of its profile dispersion of light is described as fundamental mode (TEM_{00} Gaussian distribution), the medium's nonlinear interaction is merely approached as an additional phase change, After that, the Fresnel-Kirchhoff diffraction integral is used to get the far field diffraction model. One of the significant metrics that may be taken as a result of the high temperature of the solid film or solution sample is the ratio of the change in the refractive index to the change in temperature, also known as dn/dT [16–18]. Light may be absorbed when a laser beam is sent through a sample; this causes the light to be absorbed [19]. When the laser beam has been focussed using

* Corresponding author.
E-mail address: hussain_badran@yahoo.com (H. Ali Badran).

https://doi.org/10.1016/j.rinp.2023.106858
Received 11 June 2023; Received in revised form 28 July 2023; Accepted 12 August 2023
Available online 19 August 2023

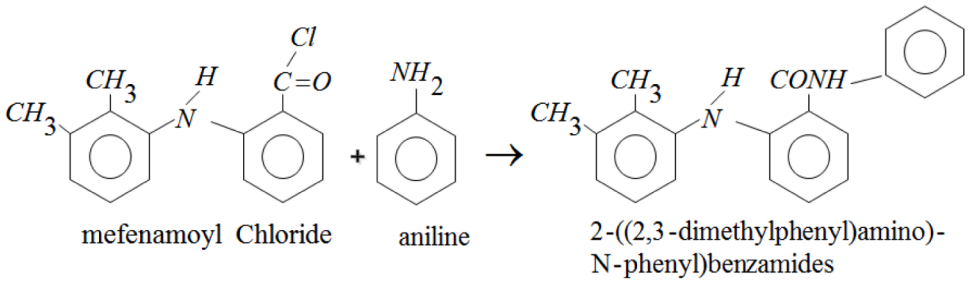

Fig. 1. The structure of the 2-NPb compound.

positive lenses, which causes a rise in the sample's temperature, the sample is positioned such that it is directly in the center of the beam [20]. Radiation-intensive investigations have been aimed toward the improvements of a variety of characteristics across a number of different materials in recent years as a direct result of the development of radiation methods over the course of the previous twenty years, such as the use of gamma ray. Ali et al.,[21] have shown quantitatively that the band gap of CR-39 narrows qualitatively with increasing gamma dosage, with the maximum being reached at 400 kGy. Qwasmeh et al.,[22] studied the effect of γ-ray on the optical properties of poly(ethylene oxide) doped with potassium iodide salt. Batool et al.,[23] studied the effect of γ-ray on the electrical properties of ultrafine iron polystyrene composites. Abdul-Kaderet et al.,[24] studied the Surface of polyethylene by electron and gamma irradiation. The influence of gamma rays on the structural and optical characteristics of polyethylene- eterephthalate (PET) polymer was investigated by Siddhartha et al. [25]. Moez et al.,[26] studied the effect of γ-ray on Optical, dielectric and FTIR of low density polyethylene (LDPE) films. The influence of gamma rays on the optical and structural properties of PC-PBT/Ag nanocomposite was investigated by Nouh et al. [27]. The influence of gamma rays on the optical and chemical characteristics of the conjugated copolymer B-co-MP was investigated by Aldaghri et al.[28]. Waldemar et al.,[29] investigated the impact that gamma rays have on the mechanical qualities of natural fibers as well as their susceptibility to biodegradation. The impact of gamma rays on a tellurium dioxide film was investigated by Khalil and Olga [30].

The goal of this research is to create a novel organic material that has strong nonlinear optical capabilities and then improve those qualities by exposing the material to gamma radiation. In order to accomplish this objective, a polymer film containing one of the organic compounds (2-NPb:PMMA film) was prepared. Polymethyl methacrylate)PMMA(is a highly adaptable polymer that has found usage in a wide variety of applications. It is utilized as a substitute for shatterproof glass, notably in Plastic Optical Fiber (POF), and it has become the resin that is most widely used in dentistry [31,32]. Since Ridley inserted the first rigid intraocular lens (IOL) in November 1949, polymethyl methacrylate has been used as one of the most biocompatible polymers used in the manufacturing of medical and surgery devices [33,34]. This application of polymethyl methacrylate dates back to when the material was originally discovered. Since that time, PMMA has served as a standard material against which succeeding IOL and hard contact lens (HCL) materials have been measured [35,36]. In addition, a substantial amount of work has been put forward in the direction of expanding the possible uses of PMMA in the realms of building and construction. In light of the fact that this substance plays a crucial part in the production of micro-devices and integrated microcircuits, a wide variety of PMMA analogs and copolymers have been synthesized and characterized in an effort to locate a resist that possesses the desirable processing properties of PMMA while also retaining a sufficient level of sensitivity [37]. In addition to having understanding of their chemical characteristics, having knowledge of the features that polymers exhibit physically would greatly boost the use of polymers. There has been a lot of research done on the material's physical qualities, including as its thermal expansion [38], heat capacity, thermal lens [39], optical swiching [40], and electrical conductivity [41]. Several methods have been developed in order to monitor the physical changes that occur in a PMMA polymer after it has been subjected to an external influence, such as radiation. These changes, in turn, have the potential to alter the performance function of the PMMA polymer.

In this work, the nonlinear refraction index (n_2) and the nonlinear absorption coefficient (β) of the pristine and irradiated polymer films were by using the Z-scan technique with solid state diode laser with an output power of 45 milli watts at 532 nm, This was done because of the sample-produced variations in a beam array that was located far away from the field of study. Seeing the Gaussian beam diffraction ring that was caused by the beam's passage through a highly nonlinear material that was thin and self-focusing. The diffraction ring profile of the polymer films is presented too. Additionally, the optical limiting action of the pure and irradiated sample was also examined.

Thin film analysis

Preparation of sample

The polymer film samples of 2-NPb PMMA were made by redissolving 6 mg from the organic compound with 2 ml of chloroform (CHF), (Sigma Aldrich) 99.99% purity, and 100 mg poly-methyl-methacrylate (Sigma Aldrich) 99.99% purity in 2 ml of CHF. Thereafter, the prepared material was left for twenty minutes on a heating plate to complete the melting process, The solution was then placed on a sonicator for fifty minutes. After complete dissolution in the solvent CHF, it was mixed with the PMMA solution and stirred once again for 25 min to produce a full adsorption and homogenous solution. Then, to prepare a thick film from the organic compound: PMMA the casting method was used, and the films were left overnight to allow the solvent to evaporate gradually from the mixture. A digital micrometer was used to measure the prepared film thickness. The polymer samples have perfect purity and a regular thickness of approximately 5 μm. all the chemical materials have been purchased from Sigma-Aldrich company, where they have high purity degrees. These chemical substances have been used without any further purifying steps being taken beforehand. Fig. 1 displays the molecular formula and structural of the 2-NPb compound prepared for the current work.

Surface morphology analysis

In this particular investigation, cesium-137 served as the gamma-ray generator. It has a longer half-life of 30.1 years, emits gamma rays at a dosage rate of 48 Rad/min, and emits energy with a value of 662 keV. Different amounts of time were spent irradiating 2-NPb:PMMA polymer film with the gamma ray, viz., one, two and three months, i.e., doses of 21, 42 and 64 KGy, respectively. After each irradiation, the image of the samples was captured using the Lenovo USB 2.0 optical microscope with UVC-DM500 Camera. Alterations in the surface profile of the films were

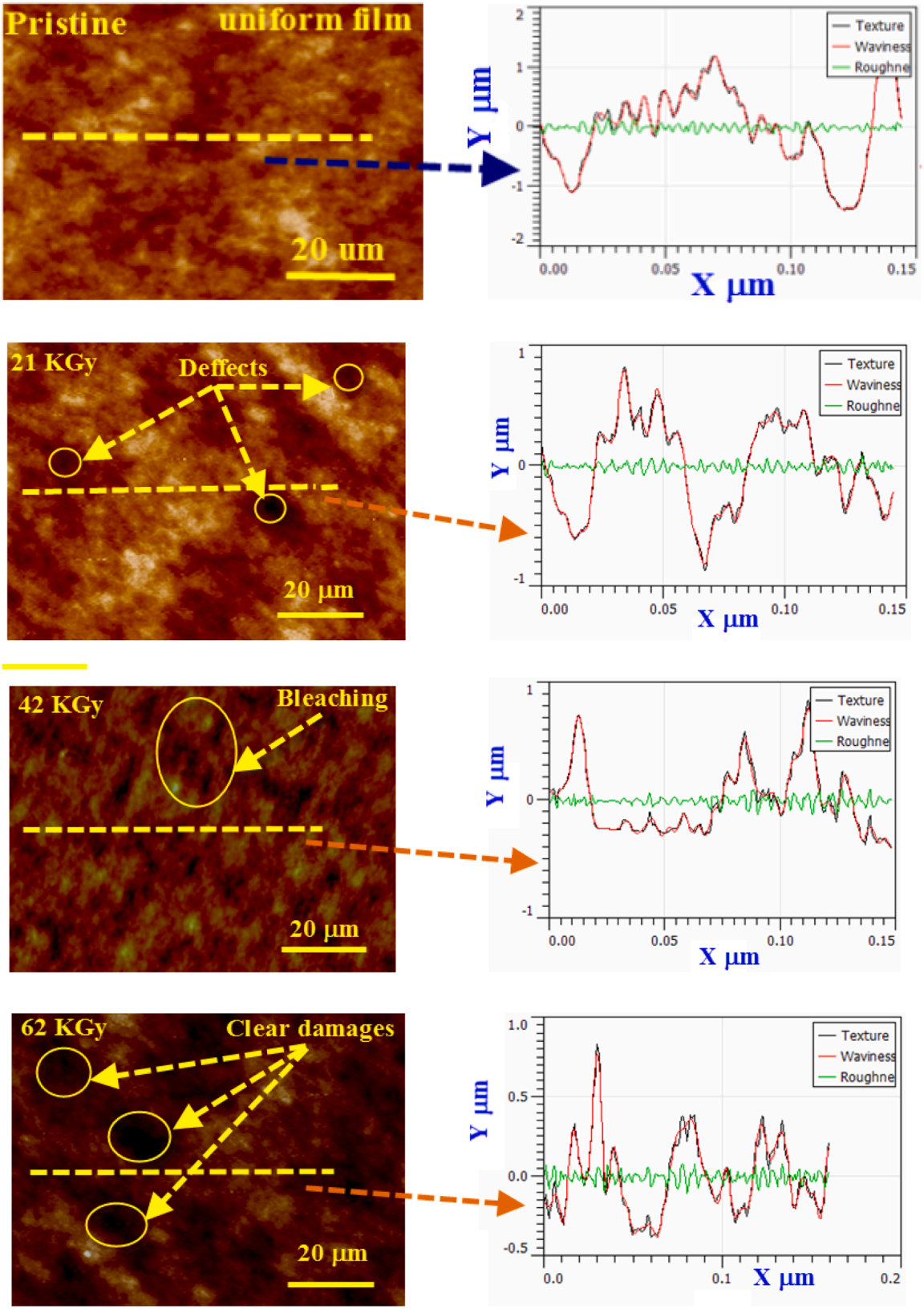

Fig.2. Surface morphology of polymer samples: (On the left side) exhibiting the optical microscope pictures of the polymer film in the pristine condition as well as under increasing - ray dosage from 21 to 62 KGy. An examination of the waviness, roughness, and texture of the whole surface of the films may be found on the right side.

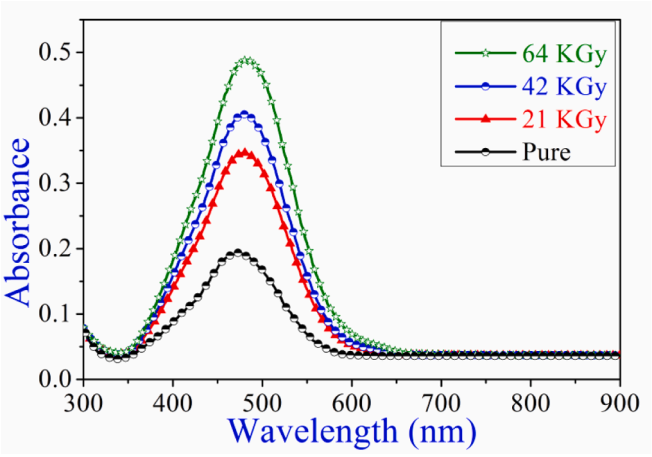

Fig. 3. A Typical absorbance spectra for the 2-NPb film exposed to various levels of the gamma radiation dose.

able to be analyzed and identified.

The study of the surface morphology of the 2-NPb: PMMA film and its characterisation for un-irradiated and irradiated films with three different doses i.e. 21, 42 and 64 KGy were examined and studied using an optical microscope with digital camera along with texture, waviness and roughen analysis of the entire surface of the films in analyzing the optical microscope images Fig. 2. Fig. 2a display surface picture of the unaltered sample as well as those of the irradiated microscopic samples. The un-irradiated sample film exhibits smoothness, homogeneity, lack of cracks, and uniformity, as can be observed in Fig. 2a. It is also possible to observe that the 2-NPb and the PMMA are spread out uniformly throughout the substrate and that there are no fractures, defects, or pinholes in the material. The sample that was irradiated with 21 KGy of gamma radiation showed flaws on its surface, and the color of the 2-NPb and PMMA changed from yellow to a yellow-orange hue as a result of the exposure. In addition to that, the pinholes can be seen clearly appearing on its surface, and they come in a variety of shapes and sizes. The 2-NPb: PMMA films was subjected to the action of gamma irradiation, which resulted in the surface alterations shown here. When the dosage was brought up to 42 KGy, the polymer film plainly displayed a black line that indicated a chemical whitening process at the surface. This was seen when the dose was raised. An increase in the whitening zone of the irradiated polymer at a dosage of 42 KGy gamma-dose is indicated by the appearance of fractures on the surface of the film as well as a dark region on the film's surface. This demonstrates that a significant portion of the irradiated polymer film has been subjected to bleaching, as shown in Fig. 2 for the irradiated film with a dosage of 64 KGy. Significant damage was discovered in the breadth of the cracked region and the formation of additional black patches as the gamma dose climbed to 64 KGy. The texture, waviness, and roughening of the whole surface of each polymeric film were analyzed in order to determine whether or not there were any changes to the surfaces of the films as the dosage rose. Beginning at the top and working our way down to the bottom, we illustrate the surface morphology profile of the portion of the original microscopic film that was chosen. In light of the trace data, it is evident that the sample's texture, waviness, and roughen scale have all become more pronounced. This finding lends credence to the hypothesis that fractures, flaws, and pinholes become more pronounced when the sample is subjected to an increasing gamma radiation. The surface profile of the picture as well as the three-dimensional analyses (texture, waviness, and roughen) of the 2-NPb film indicate the modifications in the morphology of the surface that can be seen in the optical images of the films after they have been subjected to gamma-irradiation.

Linear optical analysis

Fundamental optical band gap behavior

An organic compound of 2-NPb has been selected. In the present work, the organic compound ratio weight is 0.1 is doped the material of Poly-methyl-methacrylate (PMMA) prepared with these steps: First, the organic compound and PMMA are dissolved separately and then the solution of both the organic compound and PMMA are mixed. In addition, the mixed solution was then stirred for two hours at 60 °C using Bexco Magnetic stirrer with hot plate. The coating of the solution was ultrasonically performed on a pre-cleaned glass slide using the spin-coating technique. Afterward, the samples were allowed to dry at room temperature for two days. Fig. 3 shows the absorbance spectra distribution of samples obtained using Cecil ReflectaScan Reflectanc Spectrophotomete CE-3055 at wavelengths of 300–900 nm. It can be shown that the high value of absorption of the sample is located at 483.5 nm. The spectra of the substance film appear to remain in the same position, even after being subjected to varying amounts of gamma radiation, which causes the peak to stay in the same spot [42–44]. Nevertheless, the only limited change that was found was that the rise or the prominence of the major bands reflected the changes that took place in the organic film structure following contact with gamma irradiation. This was the only change that was detected.

The linear absorption coefficients (LAC),α_{pco}, for pristine film and irradiated 2-NPb film by gamma irradiation with different doses, namely 21, 42 and 64 KGy, were calculated by the analysis of the optical absorbance spectra, after correction for reflection, according to the using following relation [45–49]:

$$I = I_{\circ}\exp^{(-\alpha_{pco}x)}$$

Hence

$$\alpha_{pco} = 2.303/x\log\left(\frac{I}{I_{\circ}}\right) = \left(\frac{2.303}{x}\right)A' \tag{1}$$

where A' is the absorption value was calculated from absorbance, while x is sample thickness.

The incoming photons possess enough amount of energy to excite electrons from the valence band into the conduction band, which leads to a significant amount of absorption in the sample. The optical absorption edge was located using this straightforward approach, which explains the characteristics of the band structure of the film. This method was used to find the optical absorption edge. In order to carry out an inquiry into the optical absorption edge, the following relationship, which is also referred to as Tauc's Technique, was used [50,51].

$$\alpha_{pco} = \frac{a'}{h\nu}(h\nu - E_g)^{m} \tag{2}$$

where α_{pco} is LAC, a' is an energy-independent constant called the band tailing parameter [52,53] and E_g is the optical band gap. The exponent m' depends on the nature of the transition, m'= 1/2, 2, 3/2 or 1/3 for allowed direct, allowed indirect, forbidden direct or forbidden indirect transitions, respectively. Eq. (2) can be written as [54];

$$\frac{d[\ln(\alpha_{pco}h\nu)]}{d(h\nu)} = \frac{m'}{h\nu - E_g} \tag{3}$$

By calculating the value of m', one may acquire information on the kind of transition. At the point frome Eq. (3), the plot of $d[\ln(\alpha_{pco}h\nu)]/d(h\nu)$ against $h\nu$ reveals a break or discontinuity that may be seen. The band gap, denoted by E_g, is determined by the discontinuity that occurs at a certain amount of energy [55]. After plotting the curves of $\ln(\alpha_{pco}h\nu)$ against $\ln(h\nu - E_g)$ using the E_g value to calculate m' value, it was determined that the value was around 2 based on the slope of the plotted curves. As a result, the value of m that was obtained indicates that the

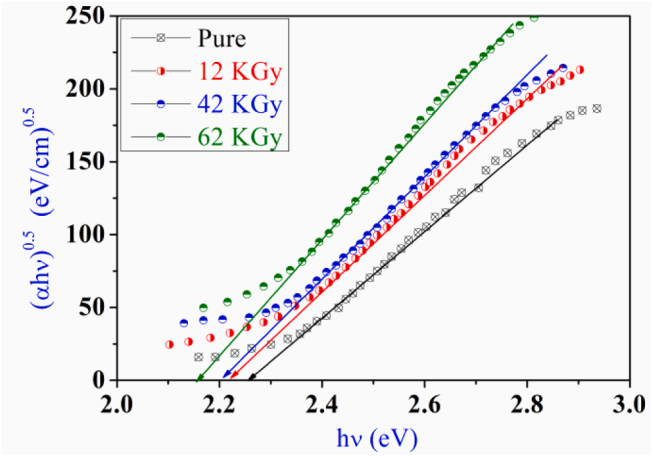

Fig. 4. $(\alpha_{pco}h\nu)^{0.5}$ as a function of $h\nu$ for different gamma radiation.

Table 1
Optical band gap of 2-NPb film for different gamma radiation.

Sample	$E_g^{ind}(eV)$
Pure	2.25
21 KGy	2.22
42 KGy	2.209
64 KGy	2.15

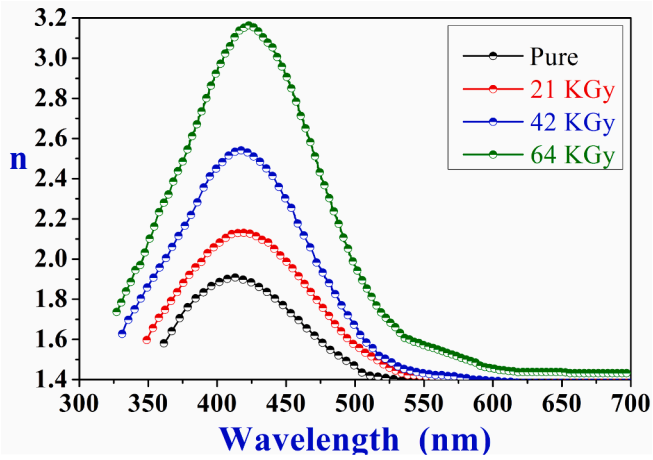

Fig. 5. The spectral behavior of n versus wavelength, for different gamma radiation dose.

basic absorption edge in the films is created by the permitted indirect transitions. During the process of transition, it is necessary to maintain the integrity of the electron-photon system's total energy as well as its momentum. The plots of $(\alpha_{pco}h\nu)^{0.5}$ and $h\nu$ are compared in Fig. 4, which may be found here. Table 1 contains the parameters that describe the indirect optical band gap E_g.

The E_g values that may be achieved via the use of this technology are appropriate for a wide variety of scientific investigations and technical applications, including piezoelectric devices and gas sensors. As can be observed from Table 1, an increase in the radiation dosage resulted in a narrowing of the films' optical band gaps. According to these findings, gamma rays are responsible for causing shrinkage of the optical absorption edge and, as a result, a change in the film's band structure. This suggests that increasing the amount of irradiation creates a greater degree of disorder, which in turn leads to a greater degree of distribution,

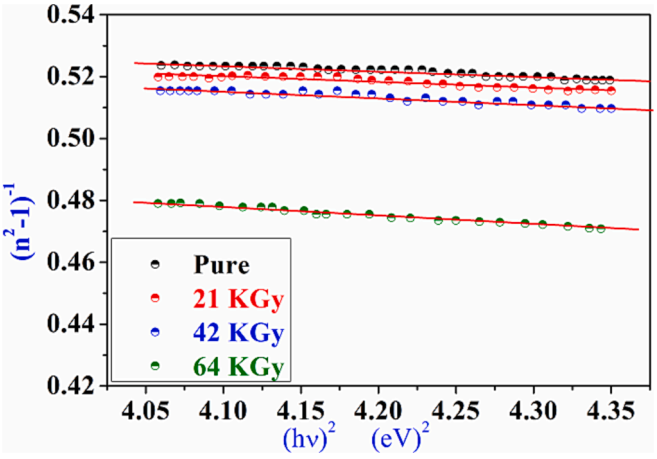

Fig. 6. $(n^2-1)^{-1}vs.(h\nu)^2$ at gamma irradiation.

which in turn leads to the production of more localized states inside the forbidden gap, which in turn leads to a reduction in the size of the optical band gap and a reduction in the band gap energy. This lends credence to the idea that defects in thin films are formed during the film creation process. It is also worth noting for discussion that decreasing the energy bandgap increases the diameter of E_g. As a result of the decrease in energy bandwidth, the band edge of the conduction band travels lower, while the band edge of the valence band rises upward as a direct consequence of the shift [56,57].

We were successful in determining the refractive index (n), by using Kramer's and Kroning's equation, of the present polymer films both in their prestine state and after being exposed to an increasing amount of gamma-ray dose, which ranged from 21 to 62 KGy. This optical index,n, may be calculated using the following equation [58,59]:

$$n = \frac{1+R}{1-R} + \sqrt{\frac{4R}{(1-R)^2} - K^2} \tag{4}$$

where R is the reflectance spectra and K is the absorption index. The plot of the spectral behavior of (n) for the 2-NPb films can be shown in Fig. 5. This figure indicates that increasing the gamma radiation of the samples that were tested led to a rise in the magnitudes of n, where the refractive index also grows as the gamma radiation level does. After reaching its greatest value at a wavelength of around 422 nm, the value of (n) begins to fall until it practically approaches a constant value. This occurs after the value of (n) achieves its maximum value. This is because, in the area of significant absorption, the incoming photon frequencies are practically identical to those of the plasma frequencies, which occurs when the wavelengths of the light are shorter. In addition, the highest coupling occurs at the point of significant absorption, which is located at around 422 nm.

Dispersion parameters

In order to establish a "dispersion energy" parameter, Wemple and Didomenico describe the frequency-dependent dielectric constant using a single oscillator [60,61]. This allows them to determine both E_d and E_o. Wemple and Di-Domenico are able to provide a fitting for the refractive index, dispersion of the films that they tested. Since dispersion is such a crucial component in both optical communication and the design of devices for spectrum dispersion, it plays an essential part in the research that is done on optical materials. While the specifics of these principles are extremely distinct from one another, they have a characteristic in common: the preponderance of evidence suggests that the behavior of solids' refractive indices may be influenced in ways that are straightforwardly explicable by crystal structure and ionicity [62]. The

Table 2
Oscillator model for samples of varying gamma irradiation with different doses.

Sample	E_o(eV)	E_d(eV)	M_{-1}	M_{-3} $(eV)^2$	n_0	λ_0(nm)	S_0 x10^{-13} (m^{-2})
Pure	7.21	12.12	1.68	0.032	1.65	167.44	6.24
14 KGy	6.68	10.86	1.62	0.036	1.63	216.32	3.58
42 KGy	5.48	8.72	1.59	0.052	1.62	229.13	3.11
64 KGy	5.01	6.52	1.30	0.051	1.59	325.28	1.37

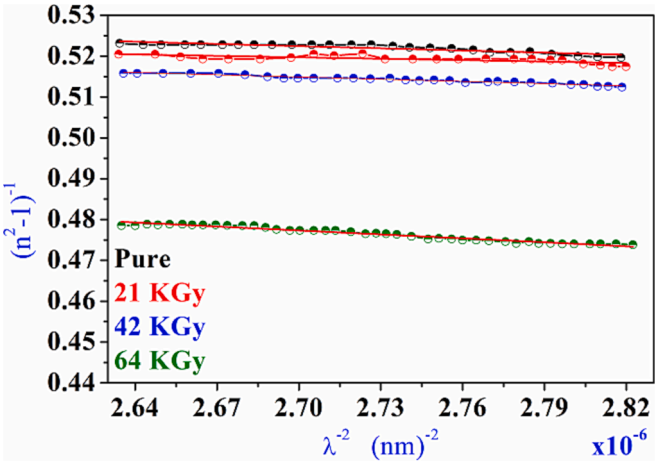

Fig. 7. $(n^2-1)^{-1}$ *vs.* λ^{-2} at gamma irradiation.

following formula illustrates the relationship that exists between the refractive index and the strength of the single oscillator below the band gap [63–65]:

$$(n^2-1)^{-1} = \frac{E_\circ}{E_d} - \frac{1}{E_0 E_d}E^2 \tag{5}$$

where E denotes the energy of a photon $E_\circ$ the energy of an oscillator, and E_d the energy of dispersion, respectively. A plot of the $(n^2-1)^{-1}$ against E^2 for pristine film and irradiated 2-NPb film by gamma irradiation with different doses is shown for our perusal in Fig. 6. It is important to note that the effective single oscillator energy, also known as $E_\circ$, or as it is frequently called, the average energy gap, E, delivers excellent results when attempting to investigate the overall band structure of the material being used. The dispersion energy, often known as E_d, is a measurement that determines the typical intensity of the interband transitions that occur inside the material. This energy, E_d, is also connected with changes in the microstructure as well as the structural order of the polymer sample that was under investigation [66]. This dispersion energy of any substance is connected to the coordinate number, the anion valency, and the ionicity of the sample in question as well. The graph illustrates this plot in its entirety. It is plainly clear that the refractive index drops as one moves toward longer wavelengths due to the influence of the film's absorption, which can be seen by moving toward longer wavelengths. E_d and $E_\circ$ values were determined from the slope and the intersection obtained by extrapolating the line to zero photon energy, and they are shown in Table 2 below. The slope and the intersection were acquired by extending the line. These two values were determined to be important in their own right.

It is possible to determine the dielectric constant of a material by using the dispersion relation of incoming photons in the calculation. Moreover, a function that extrapolates towards shorter wavelengths was used in the fitting process for the n [67]. According to the model proposed by Moss [68], the contribution of free carriers to the process of dispersion is, on the whole, rather little. This indicates that the data that correspond to the wavelength range that is below the material's absorption edge are to be utilized. In this scenario, one is in a position to apply the following relation. The characteristics of the polymer sample under investigation may be thought of as those of a single oscillator operating at high frequency and wavelength λ_0. It is possible to determine the high frequency dielectric constant by making use of the straightforward classical dispersion relation that is shown below [69].

$$\frac{n_0^2-1}{n^2-1} = 1 - \left(\frac{\lambda_0}{\lambda}\right)^2 \tag{6}$$

As can be seen in Fig. 7, when $(n^2-1)^{-1}$ was plotted against λ^{-2}, the linear component of the plot was located below the absorption edge. Table 2 provides n_0 value estimates for various film thicknesses. It is also possible to write Eq. (6) as [69]:

$$n^2-1 = \left(\frac{S_0^2\lambda_0^2}{1-(\lambda^2/\lambda_0^2)}\right) \tag{7}$$

where So represents the average strength of the oscillator, which may be found by:

$$S_0 = \frac{n_0^2-1}{\lambda_0^2} \tag{8}$$

The values for the films' So were determined by applying Eq. (7) to the equation and can be found in Table 2. It is possible to obtain the M_{-1} and M_{-3} moments of the optical spectra by using the connection [70,71].

$$E_o^2 = \frac{M_{-1}}{M_{-3}} and E_d^2 = \frac{M_{-1}^3}{M_{-3}} \tag{9}$$

The results that were obtained are shown in Table 2. As a result of the creation of the coordination complex, the M_{-1} and M_{-3} moments were different. It has been discovered that M_{-1} values drop as film γ-rays increases.

Nonlinear optical result

Self diffraction ring setup

An experiment to count the number of self induced rings is shown in Fig. 8. In this experiment technique, the 2-NPb:PMMA sample is fixed at

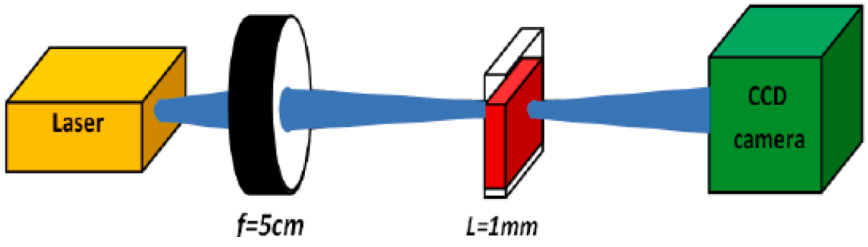

Fig. 8. Experimental set-up for counting the number of rings.

Table 3
The nonlinear parameters.

Gamma Dose (KGy)	Rings No.	ΔΦ	$n_2 \times 10^{-6}$ cm^2/W	$\Delta n \times 10^{-3}$
0	2	0.21	0.23	0.86
21	4	0.43	0.92	3.47
42	6	0.65	1.64	6.17
64	9	0.98	3.14	11.88

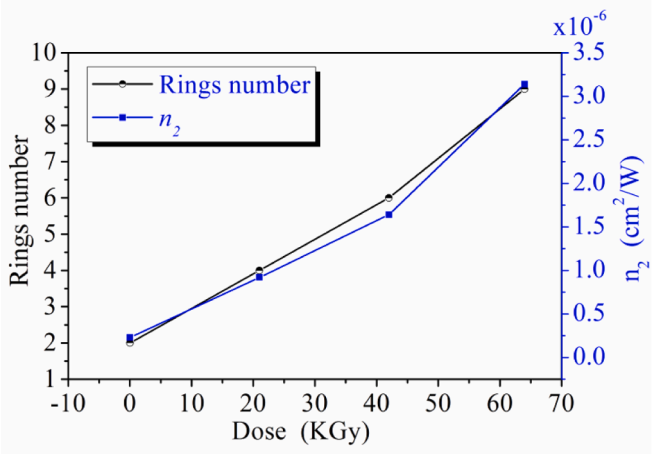

Fig. 9. n_2 as a function of rings number with different doses of γ- rays.

the focus, then the green light solid state laser (SDL) is projected to obtain diffraction rings, which in turn fall into the semitransparent screen dimension of 30 × 60 cm and then photographed by the sensitive digital CCD camera. The laser light's strength is 43mW, and its wavelength is 532 nm.

Estimation of nonlinear coefficient

Using the number of self induced rings that are shown on the screen, one may do the calculation necessary to get the nonlinear refractive index (NRX). Because the laser beam is an example of Gaussian radiation, the phase shift may be represented mathematically as [72].

$$\Delta\Phi = \Delta nkx \tag{10}$$

where $k = 2\pi/\lambda$ is the beam wave vector in a vacuum and x is the cell thickness. The relation between ΔΦ and the number of rings, N can be written as [73,74]:

$$\Delta\Phi = 2\pi N \tag{11}$$

The equation that describes both the linear and nonlinear refraction coefficients is as follows [75–77]:

$$n = n_\circ + n_2 I \tag{12}$$

where n is the overall refractive index of the material. Alternatively, Eq. (12) may be written as [78–81]:

$$n = n_\circ + \Delta nand\Delta n = n_2 I \tag{13}$$

Using Eqs. (10)–(13), the magnitudes of n_2,Δn and phase shift (ΔΦ) as seen in Table 3.

The results in Table 3 represent the behavior of n_2 and the number of self diffraction pattern with the irradiation dose. As evidenced by Table 3, that irradiation with gamma rays plays a fundamental role in improving the nonlinear optical properties of 2-NPb:PMMA films. When the sample is pure and non-radioactive, it exhibits nonlinear properties represented by the number of rings whose magnitude is 2 rings on the screen as a result of illuminating it with solid-state lasers at intensity 3.74 KW/cm^2. For the same incident intensity from a CW laser, when 2-NPb films irradiated with a dose of 21 gamma rays, the dye showed 4 rings on the screen and the value of the NRX equal to 0.92×10^{-6} cm^2/W. But when the amount of irradiation is large and within 64 KGy the number of the rings are equal to 9 rings and the value of the NRX (n_2) is within 3.14×10^{-6} cm^2/W, and here it can be said that the irradiation led to the improvement of the nonlinear optical properties (NOP) of organic compound of 2-NPb. This means that as the radiation dose is increased, the nonlinear properties improve [82], which in turn causes an increase in the number of rings appearing on the sensitive screen and the large value of the NRX. Fig. 9 presents a comparison of these metrics and explains their meaning.

The sample is heated when the basic Gaussian TEM$_{00}$ mode laser beam with a spot size of 1.2 mm passes through it, which is also when the rings show on the screen. The number of rings grows with the rising laser intensity, and this growth continues until it achieves saturation. Also, when the concentration of the solution goes up, the number of rings goes up because organic compound molecules pile up in the middle. Heat spreads over a larger area because of diffusion, which causes a lot of interference and a rise in the number of rings [83]. Fig. 10 explains the far field diffraction rings patterns of the pristine and irradiated 2-NPb:PMMA films by gamma irradiation with different doses. It is evident that for a given concentration, the number of diffraction rings rises as the irradiation dosage increases. Fig. 10 illustrates how the ring number changes as a function of the amount of ionizing radiation received.

Theoretical model

If we assume that the Gaussian beam with a wavelength λ travels through a nonlinear medium of thickness x and α_{pco} along the axis in the Z direction. We assume that the position of the beam is given within the dimension area of the system, and the complex value of the electric field passing through the sample can be expressed in the following way [83]:

$$E'(r, Z_\circ') = E(0, Z_\circ')\exp\left(-\frac{r^2}{\omega_\circ^2}\right)\exp\left(-\frac{ik_\circ n_\circ r^2}{2R}\right) \tag{14}$$

where r is the radiative coordinate, $Z_\circ'$ is the coordinate of the location within the plane of the medium, k is the wave vector in free space, $n_\circ$ is the background refractive index of the air surrounding the sample, the radius of curvature (R = 33 mm) of the wave front at the location. If we assume that the Kerr linearity occurs after the transmission of the Gaussian beam through the polymer film, then the total phase change will be expressed in an equation:

$$\varphi(r) = k\frac{n_\circ r^2}{2R} + \Delta\varphi(r) \tag{15}$$

The first term in this equation is the phase input to the beam's curve. It can be expressed by the equation below [84]:

$$\Delta\varphi(r) = k\int_{z_\circ}^{z_\circ+L}\Delta n(z, r)dz = \Delta\varphi_\circ\exp\left(-\frac{2r^2}{\omega_\circ^2}\right) \tag{16}$$

where $\Delta\varphi_\circ = k\Delta n(z_\circ, 0)L$ signifies the highest point of the beam's nonlinear phase shift. The complex electric field of the optical wave after it has traveled along the nonlinear sample is [85]:

$$E(r, Z_\circ' + L) = E(0, Z_\circ')\exp\left(-\frac{r^2}{\omega_\circ^2}\right)\exp\left(-\frac{\alpha_{pco}x}{2}\right)\exp[-i\varphi(r)] \tag{17}$$

The distribution patterns in the far-field can be obtained through the free transmission of the wave in optical space, and depending on the Fraunhofer approximation on the Kirchhoff diffraction integrally, one can get [86,87]:

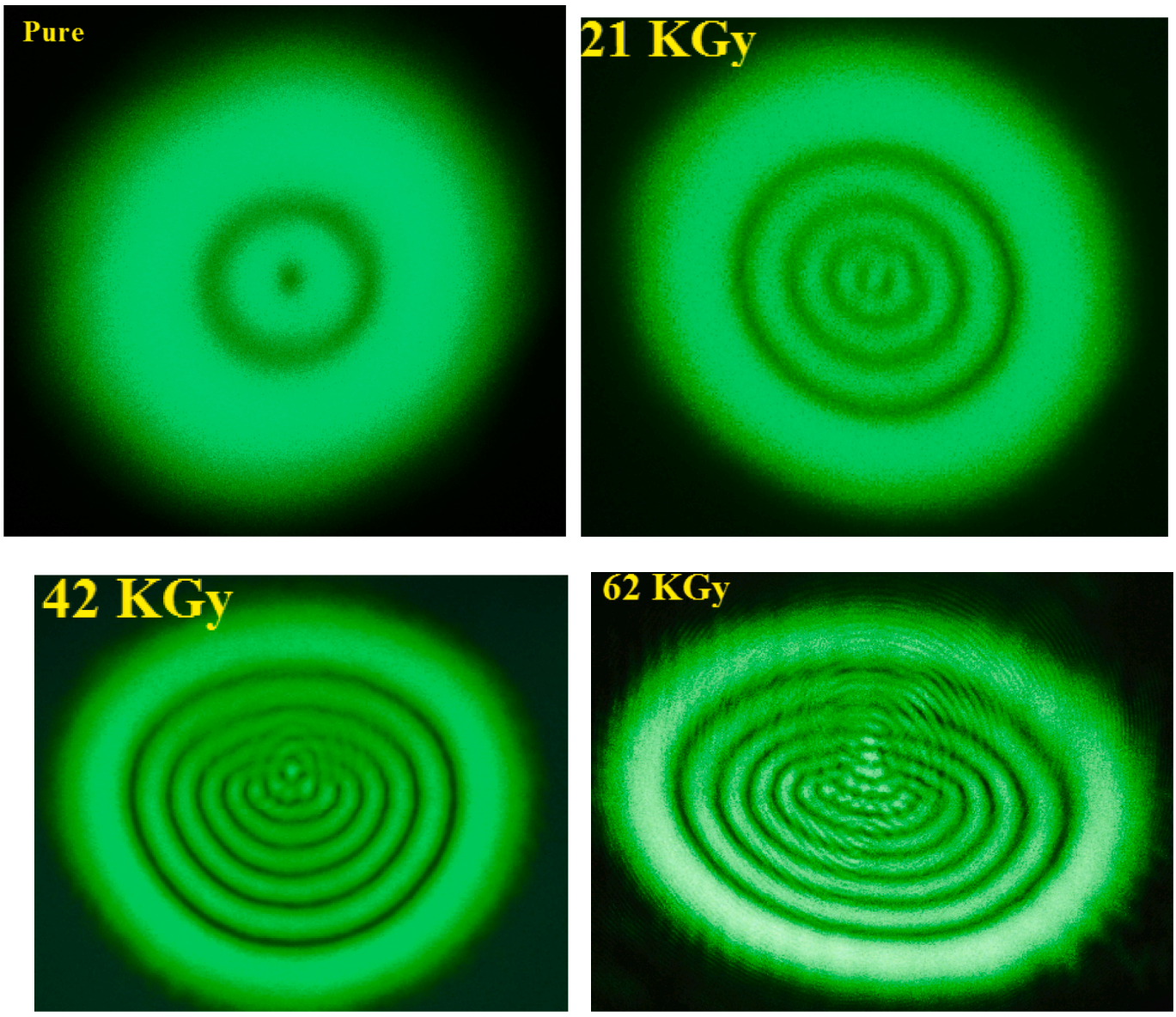

Fig. 10. The distinct ring patterns of far-field diffraction that were seen at various irradiation doses (a) 2 rings, (b) 4 rings, (c) 6 rings, (d) nine rings in the pristine film and irradiation films.

$$I(\rho) = I_{\circ}\left|\int_0^{\infty} J_{\circ}(k_{\circ}\theta r)\exp\left[-\frac{r^2}{\omega_{\circ}^2} - i\varphi(r)\right] rdr\right|^2 \tag{18}$$

where $J_{\circ}(x)$ is the zero-order Bessel function of the first kind, θ is the angle of deviation in the far field, and ρ represents the radiation coordinate in the far-field of the visible plane. $I_{\circ}$ may be expressed as follows:

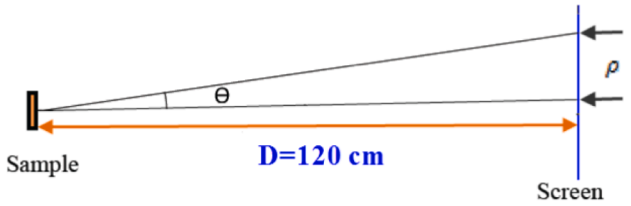

Fig.11. Experimental θ, D and ρ as they are employed in the theoretical analysis.

$$I_{\circ} = 4\pi^2\left|\frac{E(0, Z_{\circ}^{'})\exp(-\alpha_{pco}x/2)}{i\lambda D}\right|^2 \tag{19}$$

When a light beam converges, the wave front's radius of curvature will be negative, while when the same beam diverges, the wave front's radius of curvature will be positive. In general, when the beam travels through a medium that has no self-focusing (or self-defocusing), the $\Delta\varphi$ change will be negative (or positive). In each instance, the two distinct behaviors can be observed in the far-field patterns.

In the first case, when the beam diverges in a non-self-focusing nonlinear sample ($\Delta\varphi < 0 \cdot R > 0$) or in the case of the beam converging in a self-focusing nonlinear sample ($\Delta\varphi > 0 \cdot R < 0$) in these limits, the number of luminous ring patterns increase linearly with the increase in the change of nonlinear phase $N = \frac{|\Delta\varphi_{\circ}|}{2\pi}$. As for the second behavior, we get it when the transmitted beam converges through a non-self-focusing nonlinear sample ($\Delta\varphi < 0 \cdot R < 0$) or in the case of the divergence of the beam in a self-focusing nonlinear sample ($\Delta\varphi > 0 \cdot R > 0$), in which case the maximum distance of the pattern centers the lowest intensity peak in the diffraction rings [88]. The

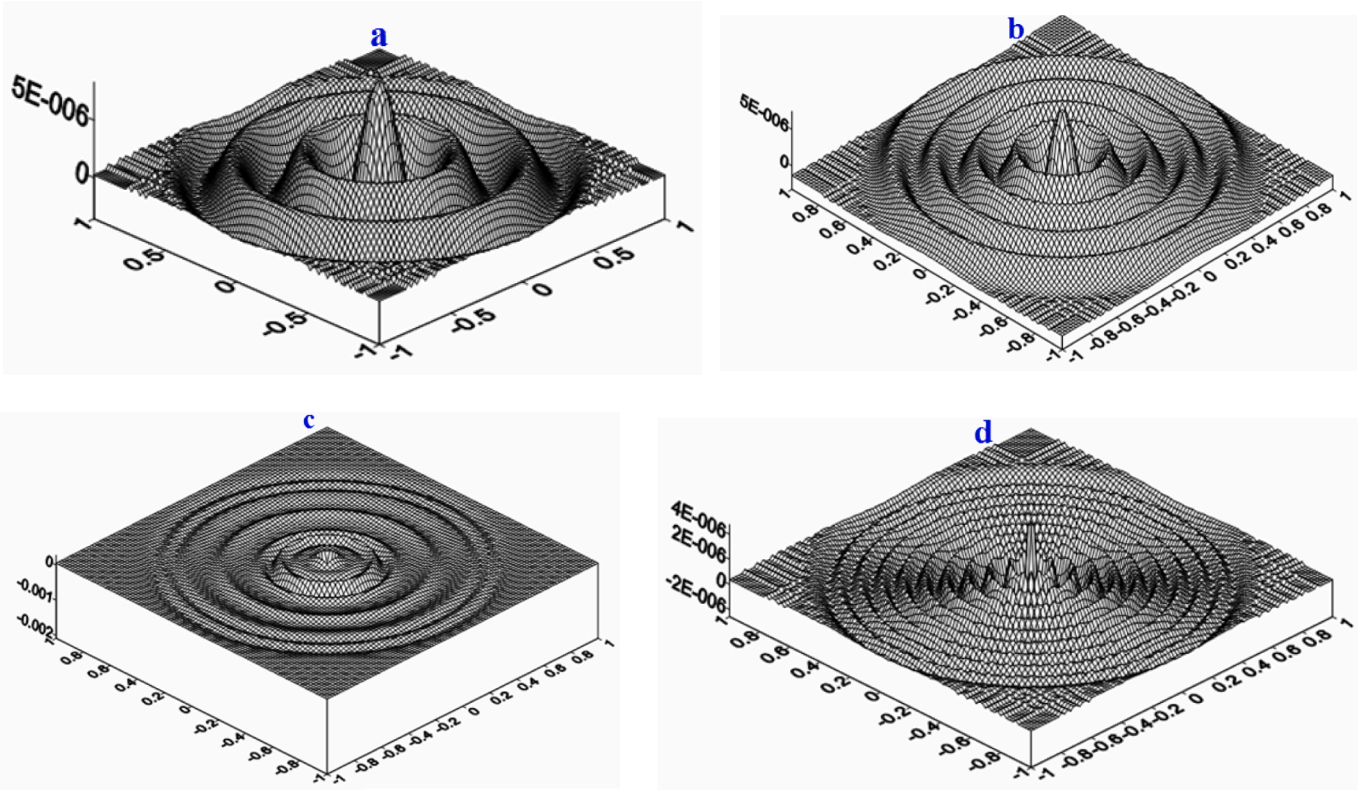

Fig. 12. 3-D distributions of far-field intensity for laser beam passing through pristine film and irradiated 2-NPb film by gamma irradiation with different doses (a) pristine film,(b) irradiated 2-NPb film with 21KGy,(c) with 42 KGy,(d) with 64 KGy.

number of luminous rings is not the same as in the first case, as it increases when the phase change increases. The data were read using the FORTRAN language of the theoretical Kirchhoff diffraction program, and the necessary data were entered to obtain the theoretical ring shape corresponding to the experimental shapes.

This theoretical model has been applied to the experimental calculations of the virgin film and irradiated 2-NPb film by γ irradiation with different doses, namely 21, 42 and 64 KGy and the coefficients listed in Fig. 11 have been used in solving Eqs. (18) and (19) to obtain theoretical rings. Simulation results of the diffraction ring patterns are shown in Fig. 12 for pristine film and irradiated 2-NPb film by gamma irradiation with different doses, namely 21, 42 and 64 KGy, respectively where it can be seen that reasonable agreement are obtained with the experimental results shown in Fig. 10.

Conclusion

In order to determine almost all of the investigated features and parameters, the refractive index,n the absorption coefficient, α_{pco} and the fundamental gap of the 2-NPb: PMMA films were used. The optical gap and the other desperation parameters ($E_\circ$,M_{-1} and E_d) of the current film samples were all reduced when the gamma radiation was increased. The spectrophotometric measurements of the absorption in the spectrum region of 300 nm- 900 nm have been necessary for the optical studies that have been conducted. According to the optical data, increasing the film's exposure to gamma rays caused the,E_g values of the tested samples to drop from 2.25 to 2.15 eV, while the first-moment, M_{-1} values dropped from 1.68 to 1.30. In the present work, the investigation of non-linear optical characteristics of 2-NPb film and irradiated samples using ^{137}Cs (γ radiation) with different doses by using self-diffraction techniques Gaussian laser output profile, using solid-state continuous wave (CW), visible laser beam at the green ray is presented. For Gaussian beams, we studied systematically, obstetrics and improvement far-field diffraction post-propagation through a 2-NPb medium (self-focused nonlinear sample). It is found that the number of self-induced diffraction rings observed in the far-field, varies as a function of gamma doses. Multiple self-diffraction rings were observed, when a beam propagates through a pristine film and irradiated 2-NPb film by gamma irradiation with different doses, namely 21, 42 and 64 KGy. The NOP of 2-NPb samples were investigated and the results showed that gamma irradiation doses lead to improve the nonlinear optical properties of 2-NPb medium very well. These results also point to the potential use of these dyes as chemical dosimeters in a certain dosage range.

CRediT authorship contribution statement

Fadhil A. Tuma: Writing – original draft, Data curation. **Mohammed T. Obeed:** Software, Data curation. **Alyaa A. Jari:** Data curation. **Hussain Ali Badran:** Writing – review & editing, Writing – original draft, Supervision, Software, Data curation. **T.A. Alaridhee:** Data curation.

Declaration of Competing Interest

The authors declare that they have no known competing financial interests or personal relationships that could have appeared to influence the work reported in this paper.

Data availability

No data was used for the research described in the article.

Acknowledgement

The authors acknowledge the Fadhil A. Tuma: Development of

polymer films, Funding acquisition.

References

[1] Poornesh P, Hegde PK, Umesh G, Manjunatha MG, Manjunatha KB, Adhikari AV. `Nonlinear optical and and optical power limiting studies on a new thiophene-based congjugated polymer in solution and solid pmma matrix. Optics Laser Technol 2010;42:230–6. https://doi.org/10.1016/j.optlastec.2009.06.018.

[2] Karimzadeh R. Spatial self-phase modulation of a laser beam propagating through liquids with self-induced natural convection flow. J Opt 2012;14:095701–9. https://doi.org/10.1088/2040-8978/14/9/095701.

[3] Junyi Y, Chunying H, Yinglin S, Jihua G. Concentration-dependent nonlinear refraction in tetrasulfonated copper phthalocyanine solution. J Opt A Pure Appl Opt 2009;11:065203. https://doi.org/10.1088/1464-4258/11/6/065203.

[4] Aiping C, Guang Y, Hua L, Peixiang L, Wenrui Z, Haiyan W. Optical limiting properties in copper oxide thin films under a higher repeitation rate femtoseconde laser. Mat Lett 2013;91:319–22. https://doi.org/10.1016/j.matlet.2012.09.111.

[5] Rekha RK, Ramalingam A. Optical nonlinear properties and optical limiting effect of metanil yellow. Am J Eng & Appl Sci 2009;2:285–91.

[6] Hussain AB, Al-Ahmad AY, Al-Mudhaffer MF, Chassib AE. Nonlinear optical responses and limiting behavior of sulfadiazine-chromotropic acid azo dye. Opt Quant Electron 2014;46:1859–67. https://doi.org/10.1007/s11082-014-0051-8.

[7] Hussain AB, Hussain FH, Ajeel KI. Nonlinear characterization of conducting polymer and electrical study for application as solar cells and its antibacterial activity. Optik 2016;127:5301. https://doi.org/10.1016/j.ijleo.2016.03.030.

[8] Alfahed RF, Al-Asadi AS, Hussain AB, Khalid IA. Structural, morphological, and Z-scan technique for a temperature-controllable chemical reaction synthesis of zinc sulfide nanoparticles. Appl Phys B 2019;125:48. https://doi.org/10.1007/s00340-019-7154-7.

[9] Hussain AB, Khalid IA, Lazim HG. Effect of nano particle sizes on the third-order optical nonlinearities and nanostructure of copolymer P3HT: PCBM thin film for organic photovoltaics. Mater Res Bull 2016;76:422–30. https://doi.org/10.1016/j.materresbull.2016.01.005.

[10] Badran HA, AL Aladil KA, Lazim HG, Al- Ahmad AY. Thermal blooming and photoluminescence characterizations of sol–gel CdO–SiO_2 with different nanocomposite. J Mater Sci Mater Electron 2016;27:2212–20. https://doi.org/10.1007/s10854-015-4013-0.

[11] Badran HA, Al-Fregi AA, Alfahed RF, Al-Asadi AS. Study of thermal lens technique and third- order nonlinear susceptibility of PMMA base containing 5′, 5″- dibromo-o-cresolsulfophthalein. J Mater Sci Mater Electron 2017;28:17288–96. https://doi.org/10.1007/s10854-017-7661-4.

[12] Hussain AB, Hanan AA, Alfahed RKF, Khalid IA. Second-order hyperpolarizability and nonlinear optical properties of novel organic compound-doped poly (O-methoxyaniline) polymer film. J Mater Sci Mater Electron 2021;32:14623–41. https://doi.org/10.1007/s10854-021-06021-2.

[13] AL-Adel KA, Badran HA. Nonlinear optical properties and diffraction ring patterns of benzo congo red. Eur J Appl Eng Sci Res 2012;1:66–72.

[14] Abdulameer I, Sattar JB, Abdalrahman A, Hussain AB. Gamma irradiation impact on the morphology and thermal blooming of sodalime glass. AIP Conf Proc 2020; 2290:050038. https://doi.org/10.1063/5.0031473.

[15] Alfahed RKF, Abdulameer I, Hussain AB, Abdalrahman A. Synthesis, optical limiting behavior, thermal blooming and nonlinear studies of dye doped polymer films. J Mater Sci Mater Electron 2020;31:13862–73. https://doi.org/10.1007/s10854-020-03946-y.

[16] Joseph SA, Hari M, Mathew S, Sharma G, Soumya HVM, Radhakrishnan P, et al. Thermal diffusivity of rhodamine 6G incorporated in silver nanofluid measured using mode-matched thermal lens technique. Opt Commun 2010;283:313–7. https://doi.org/10.1016/j.optcom.2009.10.016.

[17] Badran HA. Investigation of the nonlinear optical response of 3-(dimethylamino)-7- aminophenothiazin- 5-ium chloride dye. IOSR J Appl Phys 2012;1:33–7.

[18] Guab YZ, Lianga ZJ, Gana FX. Self-diffraction and optical limiting properties of organically modified sol–gel material containing palladium- octaisopentyloxy-phthalocyanine under cw laser illumination. Opt Mater 2001;17:471–5. https://doi.org/10.1016/S0925-3467(01)00067-2.

[19] He T, Wang C. Study on the nonlinear optical properties of three azo dyes by Z-scan measurements. J Mod Opt 2008;55:3013–20. https://doi.org/10.1080/09500340802296307.

[20] Alfahed RKF, Badran HA, Abu Talib YA, Noor AS. Investigation of third order nonlinearity of Ethidium bromide doped deoxyribonucleic acid (DNA). J Phys Conf Ser 2021;1963:012136. https://doi.org/10.1088/1742-6596/1963/1/012136.

[21] Tanu S, Sanjeev A, Shyam K, Mittal VK, Kalsi PC, Manchanda VK. Effect of gamma irradiation on the optical properties of CR-39 polymer. J Mater Sci 2007;42: 1127–30. https://doi.org/10.1007/s10853-006-0516-7.

[22] Ahmed AHQ, Batool AAS, Mohammed AT, Mou'ad AT, Ziad ME, Ruba IA, Hassan KJ. Effects of gamma irradiation on optical properties of poly(ethylene oxide) thin films with potassium iodide. J Compos Sci 2023;7(5):194. https://doi.org/10.3390/jcs7050194.

[23] Batool AAS, Ziad ME, Ruba IA, Hassan KJ, Awwad MZ. Ultrafine iron particles/polystyrene composites: effects of gamma radiation and manufacture aging on the AC electrical characterization. Radiat Eff Defects Solids 2022;177:10. https://doi.org/10.1080/10420150.2022.2105217.

[24] Abdul-Kader AM, Turos A, Radwan RM, Kelany AM. Surface free energy of ultra-high molecular weight polyethylene modified by electron and gamma irradiation. Appl Surf Sci 2009;255(17):7786–90. https://doi.org/10.1016/j.apsusc.2009.04.176.

[25] Siddhartha SA, Kapil D, Suresh Kumar R, Krishna JBM, Wahab MA. Effect of gamma radiation on the structural and optical properties of Polyethyleneterephthalate (PET) polymer. Radiat Phys Chem 2012;81(4):458–62. https://doi.org/10.1016/j.radphyschem.2011.12.023.

[26] Abdel MA, Aly SS, Elshaer YH. Effect of gamma radiation on low density polyethylene (LDPE) films: Optical, dielectric and FTIR studies. Spectrochim Acta A Mol Biomol Spectrosc 2012;93:203–7. https://doi.org/10.1016/j.saa.2012.02.031.

[27] Nouh SA, Benthami K, Samy RM, El-Hagg AA. Effect of gamma radiation on the structure and optical properties of polycarbonate-polybutylene terephthalate/silver nanocomposite films. Chem Phys Lett 2020;741(16):137123. https://doi.org/10.1016/j.cplett.2020.137123.

[28] Osamah AA, El-Badry BA, Mohammed KMA, Khalid HI. Effect of Gamma Irradiation on the Optical Properties of the Conjugated Copolymer B-co-MP. Appl Sci 2022;12(3):1606. https://doi.org/10.3390/app12031606.

[29] Waldemar M, Beata G, Jan P, Henryk W. Effects of gamma radiation on the mechanical properties of and susceptibility to biodegradation of natural fibers. Text Res J 2013;83(1):3–12. https://doi.org/10.1177/0040517512449045.

[30] Khalil A, Olga K. Gamma Radiation Dosimetry Using Tellurium Dioxide Thin Film Structures. Sensors 2002;2(8):347–55. https://doi.org/10.3390/s20800347.

[31] Dootz ER, Koran A, Graig RG, Prothet J. Comparison of the physical properties of 11 soft denture liners. Dental 1992;67:707–12. https://doi.org/10.1016/0022-3913(92)90176-b.

[32] Craig RG (Ed.), Restorative Dental Materials, 9th ed. (C. V. Mosby, St. Louis, 1993).

[33] Matthews MW, Eggleston HC, Hilmas GE.Development of a repeatedly adjustable intraocular lens. J. of Cataract & Refractive Surgery 2003;29(11):2204-2210. https://doi.org/ 10.1016/S0886-3350(03)00581-9.

[34] Peter E, John F. Assessment of the Damage in Retrieved Patellar Components. J Long Term Eff Med Implants 2010;20(1):57–72.

[35] Lee HB, Khang G, Lee JH. Polymeric Biomaterials, in Biomaterials Principles and Applications, ed by Park JB. Bronzino JD: CRC Press, USA; 2002. p. 61–6.

[36] Kohnen TMD. The variety of foldable intraocular lens materials. Journal of Cataract Refractive Surgery 1996;22:1255–9. https://doi.org/10.1016/S0886-3350(96)80079-4.

[37] Algers J, Sperr P, Egger W, Liszkay L, Kogel G, De Beardemaeker J, et al. Free volume determination of azobenzene-PMMA copolymer by a pulsed low-energy positron lifetime beam with in-situ UV illumination. Macromolecules 2004;37: 8035–42. http://hdl.handle.net/1854/LU-361979.

[38] Al-Qaradawi IY, Abdulmalik DA, Madi NK, Almaadeed M. Gamma irradiation effects on polymethyl Methacrylate. phys. stat. sol. C 2007;4(10):3727–30. https://doi.org/10.1002/pssc.200675846.

[39] Hussain AB. Thermal properties of a new dye compound measured by thermal lens effect and Z-scan Technique. Appl Phys B 2015;119:319–26. https://doi.org/10.1007/s00340-015-6068-2.

[40] Hussain AB. Thermal lens and all optical switching of new organometallic compound doped polyacrylamide gel. Results Phys 2014;4:69–72. https://doi.org/10.1016/j.rinp.2014.05.004.

[41] Inoue T, Saitooh M, Nishiyama M. J Nibon Univ Sch Dent 1993;35:252.

[42] Hussain AB, Al-Maliki A, Alfahed RKF, Ali SB, Al-Ahmad AY, Al-Saymari FA, et al. Synthesis, surface profile, nonlinear reflective index and photophysical properties of curcumin compound. J Mater Sci Mater Electron 2018;29:10890–903. https://doi.org/10.1007/s10854-018-9167-0.

[43] Badran HA, Abul-hail RC, Obeed MT. Study on effect of gamma radiation on some linear and nonlinear properties of Pyronine Y. AIP Conf Proc 2020;2290:050035. https://doi.org/10.1063/5.0027452.

[44] Obeed MT, Abul-Hail RC, Badran HA. Gamma irradiation effect on the nonlinear refractive index and optical limiting behavior of pyronine Y dye solution. Journal of Basrah Researches (Sciences) 2020;46:49–56.

[45] Lazim HG, Ajeel KI, Badran HA. The photovoltaic efficiency of the fabrication of copolymer P3HT: PCBM on different thickness nano-anatase titania as solar cell. Spectrochim Acta A Mol Biomol Spectrosc 2015;145:598–603. https://doi.org/10.1016/j.saa.2015.02.096.

[46] Kadem B, Alfahed RKF, Ahmed SA, Hussain AB. Morphological, structural, optical, and photovoltaic cell of copolymer P3HT: ICBA and P3HT:PCBM. Optik 2020;204: 164153. https://doi.org/10.1016/j.ijleo.2019.164153.

[47] Hussain AB, Abul-hail RC, Obeed MT. Study on the effect of gamma radiation on some linear and nonlinear properties of Pyronine Y. AIP Conf Proc 2020;2290: 050035.https://doi.org/10.1063/5.0027452.

[48] Badran HA. Study on Optical Constants and Refractive Index Dispersion of Neutral red Doped Polymer Film. Am J Appl Sci 2012;9:250–3. https://doi.org/10.3844/ajassp.2012.250.253.

[49] Alfahed RKF, Dheyaa A, Zahraa Y, Hussain AB, Kareem KM. Preparation and characterization of tin chloride-based polymeric composite for gamma shielding applications. Appl Radiat Isot 2023;196:110774. https://doi.org/10.1016/j.apradiso.2023.110774.

[50] Abdulah AH, Musa AA, Alfahed RKF, Hussain AB. Diffracting samples Nonlinear: optical properties and morphology for (2- hydroxyphenyl) [2-(2-methoxybenzylideneamino)- 5-methyl phenyl] telluride film. AIP Conf Proc 2020; 2290:050049. https://doi.org/10.1063/5.0027845.

[51] Ahmed SH, Akl AA. Influence of composition on optical and dispersion parameters of thermally evaporated non-crystalline $Cd_{50}S_{50-x}Se_x$ thin films. J Alloy Compd 2015;648:280–90. https://doi.org/10.1016/j. jallcom.2015.06.231.

[52] Ahmed SH, Sharma I. Dielectric properties, Optoelectrical parameters and electronic polarizability of thermally evaporated a-Pb-Se-Ge thin films. Phys B Condens Matter 2021;622:413330. https://doi.org/10.1016/j.physb.2021.413330.

[53] Ahmed SH. Studies on dielectric properties, opto-electrical parameters and electronic polarizability of thermally evaporated amorphous $Cd_{50}S_{50-x}Se_x$ thin films. J Alloy Compd 2016;671:566–78. https://doi.org/10.1016/j.jallcom.2016.02.126.

[54] Ishu S, Pankaj S, Ahmed SH. Optical properties and optoelectrical parameters of the quaternary chalcogenide amorphous Ge15SnxS35-xTe50 films. J Non Cryst Solids 2022;590:121673. https://doi.org/10.1016/j.jnoncrysol.2022.121673.

[55] Al-Fahed RKF, Alaa AR, Munaf SM, Hussain AB. Chemical Polymerization Method to Synthesize Polyaniline as a Novel Anode Catalyst in Microbial Fuel Cell. Polym Sci, Ser B 2021;63:773–80. https://doi.org/10.1134/S1560090421060026.

[56] Yakuphanoglu F. Heat treatment effect on the single oscillator parameters and optical band gap of an organic thin film. Opt Mater 2006;29:253–6. https://doi.org/10.1016/j.optmat.2005.08.033.

[57] Abeles F. Optical Properties of Solids. Amsterdam, London: North-Holland Publishing Company; 1972.

[58] Ahmed SH, Ishu S, Pankaj S. Inference of Sn addition on optical properties of the novel thermally evaporated thin a-Ge15Te50S35-xSnx films and some physical properties of their glasses. Mater Chem Phys 2023;293:126887. https://doi.org/10.1016/j.matchemphys.2022.126887.

[59] Ahmed SH, El Radaf IM. Effect of fluorine doping on the structural, optical, and electrical properties of spray deposited Sb_2O_3 thin films. Mater Sci Semicond Process 2023;160:107405. https://doi.org/10.1016/j.mssp.2023.107405.

[60] Wemple SH, DiDomenico M. Optical Dispersion and the Structure of Solids. Phys Rev Lett 1969;23:1156–60. https://doi.org/10.1103/PhysRevLett.23.1156.

[61] Wemple SH, DiDomenico M. Behavior of the electronic dielectric constant in covalent and ionic Materials. Phys Rev B 1971;3:1338–51. https://doi.org/10.1103/PhysRevB.3.1338.

[62] Jay NZ, James D.J, Richard BS. Electrical and Optical Properties of Epitaxial Films of PbS, PbSe, PbTe, and SnTe. Phys. Rev.A1965;140:330.https://doi.org/10.1103/PhysRev.140.A330.

[63] El-Denglawey A, Kamal AA, Dahshan A, Ahmed SH. Optical Characteristics of Thermally Evaporated Thin a-(Cu2ZnGe)50−xSe50+x Films. ECS J Solid State Sci Technol 2022;44(4):044006. https://doi.org/10.1149/2162-8777/ac627b.

[64] Hussain SS, Waleed AH, Hussain AB. Determination of the optical constants and optical limiting of doped malachite green thin films by the spray method. Adv Appl Sci Res 2012;3:2940–6.

[65] Ticha H, Tichy L. Semiempirical Relation Between Non-Linear Susceptibility (Refractive Index), Linear Refractive Index and Optical Gap and Its Application to Amorphous Chalcogenides. J Optoelectron Adv Mater 2002;4:381–6.

[66] Ahmed SH. Intensive linear and nonlinear optical studies of thermally evaporated amorphous thin Cu-Ge-Se-Te films. J Non Cryst Solids 2022;586:121563. https://doi.org/10.1016/j.jnoncrysol.2022.121563.

[67] Moss TS. Optical Properties of Semi-conductors, CH-2, Dispersion Theory. New York: Academic Press INC.; 1959. p. 15–33.

[68] Hasan HA, Nadia AHA, Hussain AB, Alfahed RK, Khalid IA. Effects of temperature on structural and linear/nonlinear optical properties of CdS nanoparticles film deposited by chemical reaction method. Opt Quant Electron 2023;55:555. https://doi.org/10.1007/s11082-023-04835-4.

[69] Yakuphanoglu F, Cukurovali A, Yilmaz I. Single-oscillator model and determination of optical constants *of some optical thin film materials*. Phys B**Condensed Matter** 2004;353:210–6. https://doi.org/10.1016/j.physb.2004.09.097.

[70] Hussain SS, Hussain AB, Waleed AH. Linear and nonlinear optical properties of I and NaBH4 doped Malachite green thin. Arch Appl Sci Res 2012;4:1804–10.

[71] Ahmed SH, Kamal AA, Elsaeedy HI, Alqahtani A. Optical characterization and dispersion discussions of the novel thermally evaporated thin a-S50-xGe10CdxTe40 films. Appl Phys A 2022;128:1021. https://doi.org/10.1007/s00339-022-06127-2.

[72] AL-Ahmad AY, AL-Mudhaffer MF, Badran HA, Emshary CA. Nonlinear optical and thermal properties of BCP:PMMA films determined by thermal self-diffraction. Opt Laser Technol 2013;54:72–8. https://doi.org/10.1016/j.optlastec.2013.05.009.

[73] Alfahed RKF, Hussain AB, Fouad ZR, Mohammad KK. Measurement of the thermo-optic coefficient and Ring surface profile of sulfadiazine azo dye by using milli watts cw laser beams. IOP Conf. Series. Mater Sci Eng 2020;928:072071. https://doi.org/10.1088/1757-899X/928/7/072071.

[74] Badran HA. Z-Scan Measurement for the thermo-optic Coefficient and transmitted beam Profile of1.8- Dihydroxy- Naphthalin-3, 6 (Disulfonic Acid-[2-(4-azo)]-N-5-Methyl-3- Isoxazolyl) -Benzene Sulfonamide. Adv Phys Theor Appl 2013;26:36–44.

[75] Al-Hazam HA, Alfahed RKF, Imran A, Badran HA, Shaker HS, Alsalihi AA, et al. Preparation and optoelectronic studies of the organic compound [2- (2,3- dimethyl phenylamino)- N-Phenyl benzamide] doped PMMA. J Mater Sci Mater Electron 2019;30:10284–92. https://doi.org/10.1007/s10854-019-01365-2.

[76] Hussain AB, Taha AY, Abdulkader AF, Emshary CA. preparation and study of the electrical and optical properties of a new azo dye (4-acetaminophenol-[2-(4-azo)]-4- amino dipheyl sulfone). J Ovonic Res 2012;8:161–70.

[77] Alfahed RKF, Al-Asadi AS, Al-Mudhaffer M, Badran HA. Synthesis, morphological and optical characterizations of the poly (O-toluidine) LiCl networks thin film. Opt Laser Technol 2021;133:106524. https://doi.org/10.1016/j.optlastec.2020.106524.

[78] Al-Salihi A, Salim RD, Alfahed RKF, Badran HA. Effect of Solar radiation induced and alpha particles on Nonlinear behavior of PM-355 film. IOP Conf. Series. Mater Sci Eng 2020;928:072056. https://doi.org/10.1088/1757-899X/928/7/072056.

[79] Sheik-Bahae M, Said AA, Wei T, Hagan DJ, Van Stryland EW. Sensitive measurement of optical nonlinearities using a single beam. IEEE J Quant Electron QE 1990;26:760–9.

[80] Al-Saymari FA, Hussain AB, Alaa YA, Chassib AE. Time dependent diffraction ring patterns in bromothymol blue dye doped PMMA film under irradiation with continuous wave green laser light. Indian J Phys 2013;87:1153–6. https://doi.org/10.1007/s12648-013-0334-0.

[81] R.K.F. Alfahed I. Abdulameer M.S. Majeed A.B. Hussain Photoluminescence characterizations and nonlinear optical of PM-355 nuclear track detector film by alpha- particles and laser irradiation Phys Scr 95 2020 075709 (8 pp) 10.1088/1402-4896/ab7e33.

[82] Alfahed RKF, Abdulameer I, Hussain AB, Abdalrahman A. Synthesis, optical limiting behavior, thermal blooming and nonlinear studies of dye doped polymer films, J. of Materials Science: Materials. Electronics 2020;31:13862–73. https://doi.org/10.1007/s10854-020-03946-y.

[83] Husan AS, Hussain AB, Alaa YA, Chassib AE. Experimental and Theoretical Study of the Laser Induced Diffraction Pattern in the Acid Orange 10 Dye: Polyacrylamide gel. J of Basrah Researches Sciences 2013;39:1–12.

[84] Ana BV, Kalaichelvi S. Diffraction rings due to spatial self-phase modulation in a photopolymerizable medium. J Opt A Pure Appl Opt 2009;11:125202. https://doi.org/10.1088/1464-4258/11/12/125202.

[85] Koushki E, Majles Ara MH. Comparison of the Gaussian-decomposition and the Fresnel-Kirchhoff diffraction methods in circular and elliptic Gaussian beams. Opt Commun 2011;284:5488–94. https://doi.org/10.1016/j.optcom.2011.08.028.

[86] Majles Ara MH, Dehghani Z, Sahraei R, Daneshfar A, Javadi Z, Divsar F. Diffraction patterns and nonlinear optical properties of gold nanoparticles. J Quant Spectrosc Radiat Transf 2012;113:366–72. https://doi.org/10.1016/j.jqsrt.2011.12.006.

[87] Robertson J, Milsom P, Duignan J, Bourhill G. Spatial redistribution of energy in a nanosecond laser pulse by an organic optical limiter. Opt Lett 2000;25:1258–60. https://doi.org/10.1364/OL.25.001258.

[88] Deng L, He K, Zhou T, Li C. Formation and evolution of far-field diffraction patterns of divergent and convergent Gaussian beams passing through self-focusing and self-defocusing media. J Opt A Pure Appl Opt 2005;7:409–15. https://doi.org/10.1088/1464-4258/7/8/011.